

# Improved Core-Loss Calculation for Magnetic Components Employed in Power Electronic Systems

**Journal Article****Author(s):**

Mühlethaler, Jonas; Biela, Jürgen ; Kolar, Johann W. ; Ecklebe, Andreas

**Publication date:**

2012-02

**Permanent link:**

<https://doi.org/10.3929/ethz-b-000039268>

**Rights / license:**

In Copyright - Non-Commercial Use Permitted

**Originally published in:**

IEEE Transactions on Power Electronics 27(2), <https://doi.org/10.1109/TPEL.2011.2162252>

# Improved Core Loss Calculation for Magnetic Components Employed in Power Electronic Systems

Jonas Mühlethaler, *Student Member, IEEE*, Jürgen Biela *Member, IEEE*, Johann Walter Kolar *Fellow, IEEE*, and Andreas Ecklebe *Member, IEEE*

**Abstract**—In modern power electronic systems voltages across inductors or transformers generally show rectangular shapes, including periods of zero voltage. In the stage of zero applied voltage (constant flux) core losses are not necessarily zero. At the beginning of a period of constant flux losses still occur in the material. This is due to relaxation processes. A physical explanation about magnetic relaxation is given and a new core loss modeling approach that takes such relaxation effects into consideration is introduced. The new loss model is called i<sup>2</sup>GSE and has been verified experimentally.

**Index Terms**—Core Losses, Ferrite, Steinmetz, Relaxation, Dual Active Bridge.

## I. INTRODUCTION

In modern power electronic systems, voltages across inductors or transformers generally show rectangular shapes as illustrated in Fig. 1. The voltage across an inductor or transformer can be positive, negative or zero. This results in the flux in the core ramping up, ramping down or remaining constant.

Core losses need to be determined for the design of inductive components. The most used equation that characterizes core losses is the power equation [1]

$$P_v = k f^\alpha \hat{B}^\beta \quad (1)$$

where  $\hat{B}$  is the peak induction of a sinusoidal excitation with frequency  $f$ ,  $P_v$  is the time-average power loss per unit volume, and  $k$ ,  $\alpha$ ,  $\beta$  are material parameters. The equation is called the Steinmetz Equation (after Charles P. Steinmetz). The material parameters  $k$ ,  $\alpha$ , and  $\beta$  are accordingly referred to as the Steinmetz parameters. They are valid for a limited frequency and flux density range. The major drawback of the Steinmetz Equation is that it is only valid for sinusoidal excitation. This is a huge drawback, because, as stated above, in power electronic applications the material is usually exposed to non-sinusoidal flux waveforms.

To overcome this limitation and determine losses for a wider variety of waveforms, different approaches have been developed. The approaches can be classified into the following categories:

- 1) Improvements of the Steinmetz Equation (1): for instance, the analysis in [2] is motivated by the fact that the

J. Mühlethaler and J. W. Kolar are with the Power Electronic Systems Laboratory, ETH Zurich, www.pes.ee.ethz.ch, Email: muehlethaler@lem.ee.ethz.ch and kolar@lem.ee.ethz.ch

J. Biela is with the Laboratory for High Power Electronic Systems, ETH Zürich, www.hpe.ee.ethz.ch, Email: j.biela@ethz.ch

A. Ecklebe is with ABB Switzerland Ltd., Corporate Research, CH-5405 Baden-Dättwil, Email: andreas.ecklebe@ch.abb.com

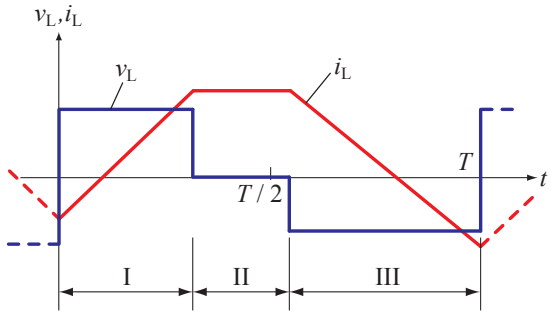


Fig. 1. Typical voltage/current waveform of magnetic components employed in power electronic systems. Phase I: positive voltage; phase II: zero voltage; phase III: negative voltage.

loss due to domain wall motion has a direct dependency of  $dB/dt$ . As a result, a modified Steinmetz Equation is proposed. In [3] the approach is further improved and in [4] a method how to deal with minor hysteresis loops is presented and some minor changes on the equation are made. The approach of [2], [3], and [4] leads to the improved Generalized Steinmetz Equation (iGSE)

$$P_v = \frac{1}{T} \int_0^T k_i \left| \frac{dB}{dt} \right|^\alpha (\Delta B)^{\beta-\alpha} dt \quad (2)$$

where  $\Delta B$  is peak-to-peak flux density and

$$k_i = \frac{k}{(2\pi)^{\alpha-1} \int_0^{2\pi} |\cos \theta|^\alpha 2^{\beta-\alpha} d\theta}. \quad (3)$$

The parameters  $k$ ,  $\alpha$ , and  $\beta$  are the same parameters as used in the Steinmetz Equation (1). By use of the iGSE losses of any flux waveform can be calculated, without requiring extra characterization of material parameters beyond those for the Steinmetz Equation. This approach is widely applied [5], [6].

- 2) Calculation of the losses with a loss map that is based on measurements. This loss map stores the loss information for different operating points, each described by the flux density ripple  $\Delta B$ , the frequency  $f$ , the temperature  $T$ , and a DC bias  $H_{DC}$  (e.g. in [7]–[9]).
- 3) Methods to determine core losses based on breaking up the total loss into loss components, i.e. hysteresis losses, classical eddy current losses, and residual losses [10], [11].
- 4) Hysteresis models such as Preisach and Jiles-Atherton used for calculating core losses.

In the categories 1 and 2 an energy loss is assigned to each section of the voltage / current waveform as illustrated in Fig. 1 (e.g. via an equation as (2) or via a loss map), and these losses are summed-up to calculate the power loss occurring in the core. This approach has e.g. been implemented in [12].

In most of the previous publications, the phase where the voltage across the magnetic component is zero has not been discussed. It has been implicitly assumed that no losses occur when the flux remains constant. However, as measurements show, this is not a valid simplification. At the beginning of a period of constant flux, losses still occur in the material. In the publication [13] about core loss modeling, a loss increase during zero voltage periods has been observed, however, no explanation or modeling approach is given.

This work hypothesizes that this loss increase is due to relaxation processes in the magnetic core material. In accordance with this hypothesis, a new model is proposed that considers relaxation processes when calculating core losses.

A core loss measurement test setup has been built to analyze core losses under general flux waveform excitations. The test system is presented in **Section II**. In **Section III** a brief introduction to magnetic relaxation is given. In **Section IV**, **V**, and **VI** a new loss model is derived that substantially improves core loss calculation by taking relaxation processes into consideration. In **Section VII** an easy-to-follow example is given to illustrate how the new model can be applied. Before concluding the work, in **Section VIII** a short discussion of the behavior of different materials is given.

## II. TEST SETUP TO MEASURE CORE LOSSES

In order to perform core loss measurements the best measurement technique has to be selected first. In [14] different methods are compared. The B-H Loop Measurement has been evaluated as the most suitable. Amongst other advantages, this technique offers rapid measurement (compared to other methods, e.g. calorimetric measurements) and a good accuracy. Furthermore, copper losses are excluded from the measurement. The principle is as follows: two windings are placed around the Core Under Test (CUT). The sense winding (secondary winding) voltage  $v$  is integrated to sense the core flux density  $B$

$$B(t) = \frac{1}{N_2 \cdot A_e} \int_0^t v(\tau) d\tau \quad (4)$$

where  $N_2$  is the number of sense winding turns and  $A_e$  is the effective core cross section of the CUT. The current in the excitation winding (primary winding) is proportional to the magnetic field strength  $H$

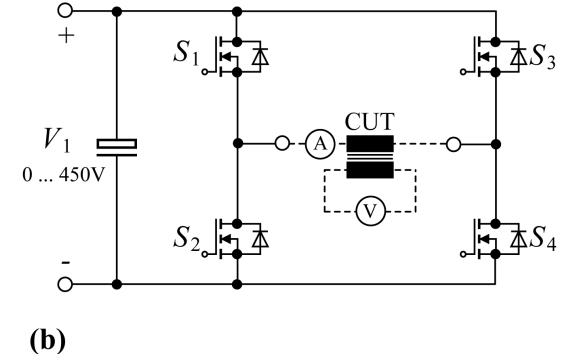
$$H(t) = \frac{N_1 \cdot i(t)}{l_e} \quad (5)$$

where  $N_1$  is the number of excitation winding turns and  $l_e$  is the effective magnetic path length of the CUT. The loss per unit volume is then the enclosed area of the B-H loop multiplied by the frequency  $f$

$$\frac{P}{V} = f \oint H dB. \quad (6)$$



(a)



(b)

Fig. 2. Test setup (a) photograph, (b) simplified schematic.

The selected approach is widely used [4], [8], [15], [16]. The built test system consists of a power stage, a power supply, an oscilloscope and a heating chamber. It is controlled by a MATLAB program running on the oscilloscope under Microsoft Windows. In Fig. 2 a photograph (a) and the simplified schematic (b) of the power stage are shown. The power stage is capable of a maximum input voltage of 450 V, output current of 25 A and a switching frequency of up to 200 kHz. The test setup allows application of a general rectangular voltage shape across the CUT that leads to a triangular or trapezoidal current shape including a DC bias (if desired).

The reader is referred to [17] for more information about the test setup, including a detailed accuracy analysis of the loss measurement.

## III. RELAXATION PROCESSES IN MAGNETIC MATERIALS

As already mentioned in the introduction, during the phase of constant flux (where the voltage across the magnetic component is zero) losses still occur in the core material. A literature survey led to the conclusion that this is due to relaxation processes in the magnetic core material. In this section, first measurements are presented that illustrate magnetic relaxation. Further, an attempt to theoretically explain the effect is given, and, with it, the resulting shape of a B-H loop for trapezoidal flux waveform is analyzed.

### A. Measurement Results

According to (2), the energy loss would only depend on the magnitude and the slope of the flux, and consequently, there should be no loss during periods of constant flux (zero

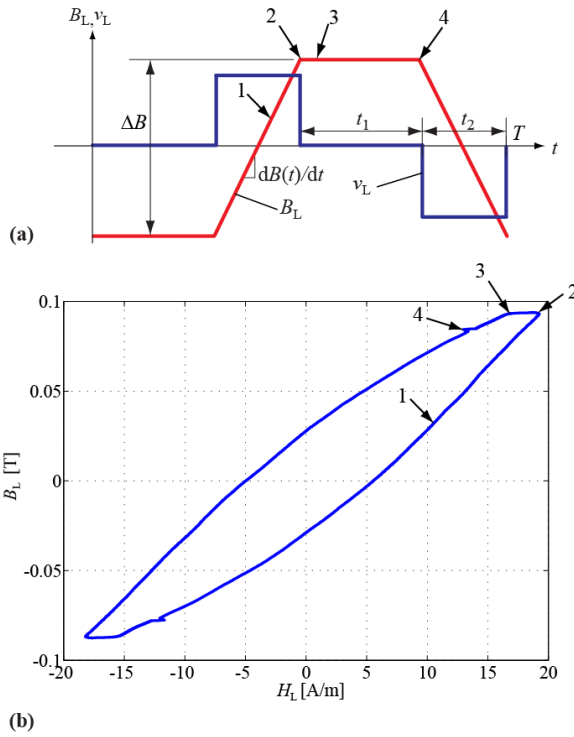


Fig. 3. (a) Voltage and flux density waveforms. (b) B-H loop to illustrate magnetic relaxation under trapezoidal flux shape condition.

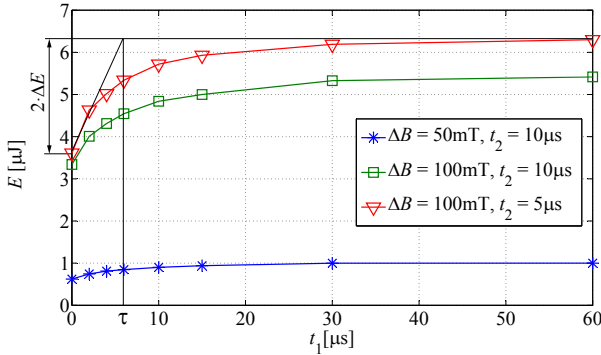


Fig. 4. Measurement results measured on ferrite EPCOS N87 (R42, B64290L22X87 [18]); temperature = 25 °C. It is further illustrated how  $\tau$  according to (18) can be extracted.

voltage). Measurements on waveforms as illustrated in Fig. 3(a) have been performed to investigate this. Fig. 4 shows the corresponding measurement results. The CUT is made of ferrite EPCOS N87 (size R42). According to (2), the duration of  $t_1$  should not influence the energy loss per cycle, but, as can be seen, increasing  $t_1$  has a substantial influence on the energy loss per cycle. In particular, a change in  $t_1$  at low values of  $t_1$  influences the dissipated loss. For larger values of  $t_1$ , the core material has time to reach its equilibrium state and no increase in losses can be observed when  $t_1$  is further increased.

Different experiments have been conducted to confirm that this effect is not due to an imperfection of the measurement setup. One could mainly think of two sources of error:

- 1) The effect of a small exponential change of current due to a residual voltage across the inductor in the "zero"

voltage time intervals, i.e. an effect related to the CUT excitation.

- 2) An error in measurements due to limited measurement capabilities of the probes, i.e. an effect related to the measurement equipment used.

The following experiments have been conducted to make sure that none of these error sources led to the observed loss increase:

- 1) A resistor has been connected in series with the primary winding, i.e. the effect of an exponential change of the current due to a voltage drop across the inductor in the "zero" voltage time intervals has been deliberately increased. A resistor of 10 Ω has been chosen as this value is certainly higher than the residual resistance of the setup (for instance, the on-resistance of one MOSFET (IXYS IXFB82N60P) is only  $R_{DS(on)} = 75\text{ m}\Omega$  at  $T_j = 25^\circ\text{C}$ ;  $I_D = 41\text{ A}$ ). The excitation voltage has been accordingly adjusted to have the same magnetic operating point. The same core loss increase in the "zero" voltage time interval has been observed as without an additional resistor, which indicates that the effect is not coming from an improper CUT excitation.
- 2) The current probe LeCroy AP015 has with 50 MHz the lowest bandwidth of the measurement equipment used. This is enough to measure the effect observed in Fig. 4. Generally, according to the accuracy analysis in [17], accurate measurement results are expected for operating points with frequencies / flux densities such as presented in Fig. 4. However, to confirm this, a simple comparative measurement has been performed to verify that the effect is not originating in the limitations of the voltage and current probes. For a limited temperature range it can be approximated that the relative change of the core temperature is proportional to the losses occurring in the core. According to this, the core losses can be observed by measuring the core temperature. The same loss increase in the zero voltage time intervals as illustrated in Fig. 4 could be observed by this simple measurement. This comparative measurement indicates that the effect is not coming from the measurement equipment used.

Last but not least, the fact that this effect has been also observed by another research group [13] greatly increases the credibility of the result.

Concluding, at the beginning of the phase of constant flux (where the voltage across the magnetic component is zero) losses still occur. Based on a literature survey, it is hypothesized that this is because of relaxation processes in the magnetic core material. Next, a brief introduction about magnetic relaxation is given.

### B. Theory of Relaxation Effects

There are basically three physical loss sources: (static) hysteresis losses, eddy-current losses, and a third loss component which is often referred to as residual losses. Hysteresis losses are linear with the frequency  $f$  (rate-independent B-H loop). Eddy-current losses occur because of an induced current due

to the changing magnetic field, and are strongly depend on the material conductivity and the core geometry. The residual losses are, according to [10], due to relaxation processes: if the thermal equilibrium of a magnetic system changes, the system progressively moves towards the new thermal equilibrium condition. When the magnetization changes rapidly, as for example is the case in high-frequency or pulsed field applications, such relaxation processes become very important.

The *Landau-Lifshitz* Equation describes qualitatively the dynamics of the magnetic relaxation processes. This is a phenomenological equation that combines all processes that are involved in magnetic relaxation. The equation follows directly from equating the rate of change of the angular momentum  $L$  to the torque  $M \times H$  reduced by a frictional term that is directed opposite to the direction of motion [10]:

$$\frac{dM}{dt} = \gamma M \times H - \Lambda M \times (M \times H)/M^2, \quad (7)$$

where  $\gamma = ge/2mc$  is the magnetomechanical ratio  $M/L$ ,  $M$  is the magnetization vector,  $H$  the magnetic field vector, and  $\Lambda$  is called the relaxation frequency. It describes how the system progressively moves towards the new thermal equilibrium. The equilibrium is achieved by rearranging the magnetic domain structures to reach states of lower energy. The relaxation process limits the speed of flux change, hence the B-H loops becomes rate-dependent. Several physical processes are contributing simultaneously to magnetic relaxation. The interested reader is referred to [10], [19], [20] for more information.

Concluding, due to *magnetic relaxation*, the magnetization may change even when the applied field is constant (the magnetization is delayed). Consequently, a residual energy loss still occurs in the period of a constant applied field. Furthermore, the shape of the hysteresis loop is changed depending on the rate of change of the applied field (rate-dependent loop). An analysis of the impact of *magnetic relaxation* to a trapezoidal flux shape now follows.

### C. Shape of B-H Loop for Trapezoidal Flux Waveforms

A B-H loop under trapezoidal flux waveform condition has been measured to gain a better comprehension of why the losses increase when the duration of the zero voltage period is increased. The CUT is a toroid core R42 made of ferrite EPCOS N87. In Fig. 3(a) the flux waveform, and in Fig. 3(b) the corresponding B-H loop are plotted. The B-H loop always traverses counterclockwise. The different instants (cf. numbers in Fig. 3(a) and (b)) are now discussed step-by-step:

- 1) A constant voltage at the CUT primary winding results in a time linear flux increase.
- 2) The CUT primary voltage is set to zero; as a consequence the flux is frozen ( $dB/dt = 0$ ). However, the material has not yet reached its thermal equilibrium. The magnetic field strength  $H$  declines to move towards the new thermal equilibrium and therewith reaches a state of lower energy. This can also be observed in the current (the current declines accordingly).
- 3) This point is reached approximately  $24\ \mu s$  after point 2. It is the point of the new thermal equilibrium.

- 4) This point is reached approximately  $200\ \mu s$  after point 3. The demagnetization in the zero voltage period is due to the small voltage drop over the on-resistance of the MOSFETs and copper resistance of the inductor primary winding. This demagnetization follows a different time constant than the demagnetization due to relaxation losses (cf. the approximately same distance 2-3 and 3-4, but the different time scale). At point 4 a negative voltage is applied to the CUT. The small buckle in the B-H loop is due to small capacitive currents at the switching instant.

The period between point 2 and 3 obviously increases the area of the B-H loop, and therewith increases the core losses. The loop area increases as a function of the duration  $t_1$ . After the thermal equilibrium is reached (in the above example after approximately  $24\ \mu s$ ) the loss increase becomes (almost) zero. In the next section more measurements are presented to find a method to include this effect into an existing core loss model.

## IV. MODEL DERIVATION 1: TRAPEZOIDAL FLUX WAVEFORM

Losses can be calculated with (2), without requiring extra characterization of material parameters beyond the parameters for the Steinmetz Equation. The Steinmetz parameters are often given by core manufacturers, hence core loss modeling is possible without performing extensive measurements. However, the approach has some drawbacks. First, it neglects the fact that core losses may vary under DC bias condition. This is discussed in [17], where a graph showing the dependency of the Steinmetz parameters ( $\alpha$ ,  $\beta$  and  $k$ ) on premagnetization is introduced. With it, losses can be calculated via the Steinmetz Equation (1) or the iGSE (2) using appropriate Steinmetz parameters. Another source of inaccuracy is that relaxation effects are not taken into consideration. As approach (2) is very often discussed in literature and often applied for designing magnetic components, improving this method would have the most practical use. Furthermore, in [6] it has been evaluated as the most accurate state-of-the-art loss model based on Steinmetz parameters. For this two reasons, in the following discussion the iGSE will be extended to consider relaxation losses as well.

When plot the losses with logarithmic axes, where the x-axis represents the frequency and the y-axis represents the power loss, an approximately straight line is drawn. This is because the losses follow a power function as e.g. the law stated in (1) is. The parameter  $\alpha$  of (1) represents the slope of the curve in the plot. In Fig. 5 such plots are given for few operating points. Instead of the frequency  $f$ ,  $dB/dt$  has been used as x-axis, which, for symmetric triangular or trapezoidal flux waveforms, is directly proportional to the frequency  $f$ . The time  $t_1$  is defined as in Fig. 3 ( $t_1 = 0$  leads to a triangular flux waveform). As can be seen in Fig. 5, when a long zero voltage phase is added between two voltage pulses (having a flux waveform as given in Fig. 3) the loss still follows a power function with variable  $dB/dt$  (the losses are still represented by an approximately straight line). The same conclusion can be made when keeping  $dB/dt$  constant and varying  $\Delta B$ , hence,

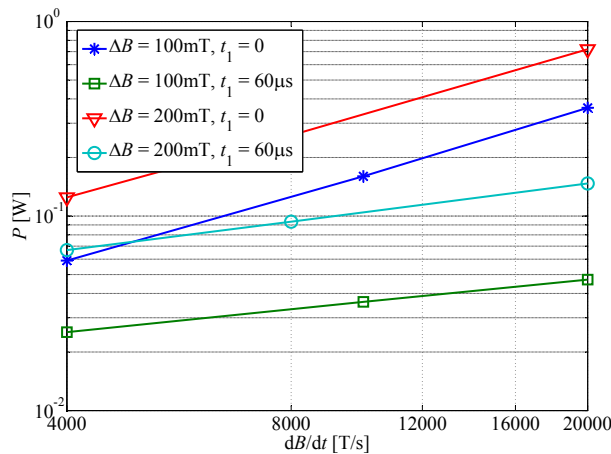
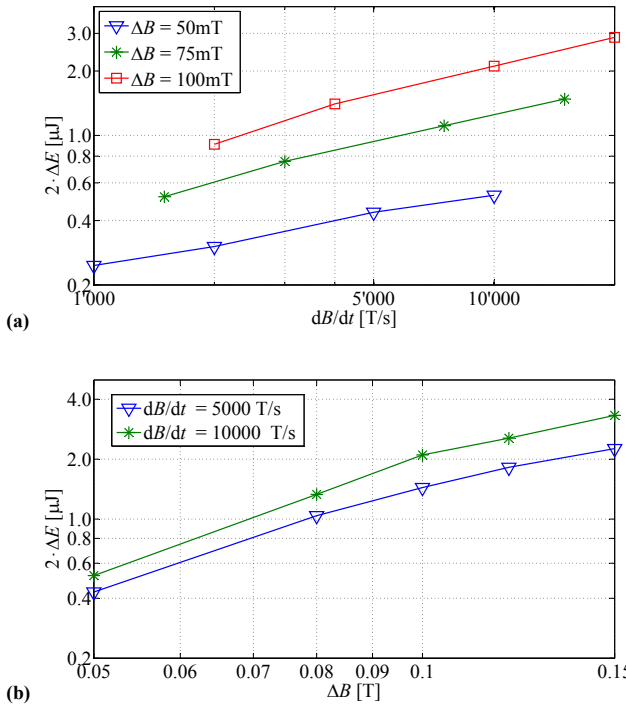


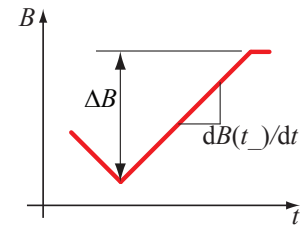
Fig. 5. Core Loss (ferrite N87; measured on R42 core); temperature = 25 °C.

Fig. 6. Measured values of  $2 \cdot \Delta E$  (ferrite N87; measured on R42 core); temperature = 25 °C.

the use of a power function with variable  $\Delta B$  is justified as well.

It should be pointed out that when a (long) zero voltage interval ( $t_1 \neq 0$ ) is present the average power loss decreases (cf. Fig. 5). There is no discrepancy with the observation in Fig. 4, where an *energy loss per cycle* increase has been observed. When having a zero voltage interval the energy loss per cycle increases, but the period increases as well and leads to a lower average power loss.

The approach of (2) will now be extended by taking relaxation effects into consideration. This is done by adding a new additional term that represents the relaxation effect of a transition to zero voltage. As can be seen in Fig. 4, the energy

Fig. 7. Definition of  $dB(t_-)/dt$  and  $\Delta B$ .

loss increase due to the zero voltage interval can be modeled with the exponential equation

$$E = \Delta E \left( 1 - e^{-\frac{t_1}{\tau}} \right), \quad (8)$$

where  $\Delta E$  is the maximum energy loss increase (which occurs, when the magnetic material has enough time to reach the new thermal equilibrium),  $\tau$  is the relaxation time that has to be further determined, and  $t_1$  is the duration of the constant flux (zero applied voltage) phase. The exponential behavior is typical for relaxation processes. Measurements have shown that  $\tau$  can be considered to be a constant parameter for a given core material that does not change for different operating points. The increase of energy loss per cycle in measurements on waveforms illustrated in Fig. 3(a) leads to twice  $\Delta E$ , since there are two transitions to zero voltage. Consequently, in Fig. 4 the loss increase is labeled as  $2 \cdot \Delta E$ . Different measurements on waveforms as illustrated in Fig. 3(a) have been conducted to determine a formula to describe  $\Delta E$ . The corresponding results are given in Fig. 6, where measured values of  $2 \cdot \Delta E$  for different operating points are plotted. In Fig. 6(a)  $dB/dt$  has been used as x-axis and in Fig. 6(b)  $\Delta B$  has been chosen for the x-axis. In both cases approximately parallel straight lines are drawn, i.e.  $2 \cdot \Delta E$  (approximately) follows a power function with variables  $dB/dt$  and  $\Delta B$ . Hence,  $\Delta E$  of one transition to zero voltage can be described by a power function with variables  $\Delta B$  and  $dB(t_-)/dt$ , where  $\Delta B$  and  $dB(t_-)/dt$  define the flux density waveform before this transition to zero voltage as illustrated in Fig. 7. As a consequence, the following power function can be defined for  $\Delta E$ :

$$\Delta E = k_r \left| \frac{d}{dt} B(t_-) \right|^{\alpha_r} (\Delta B)^{\beta_r}, \quad (9)$$

where  $\alpha_r$ ,  $\beta_r$ , and  $k_r$  are new model parameters which have to be determined empirically. With (9), the relaxation losses of a transition to zero voltage can be determined according to the antecedent flux density slope  $dB(t_-)/dt$  and the antecedent flux density peak-to-peak value  $\Delta B$ . Accordingly, when the flux density reaches and remains at zero as occurs e.g. in a buck converter that is operating in discontinuous conduction mode, relaxation losses have to be taken into consideration as well. However, the losses *may* (slightly) differ in this situation because the antecedent flux density is DC biased. This DC level of the antecedent flux density has not been part of investigation of the present work and could be investigated as part of a future work.

Concluding, (2) has been extended by an additional term that describes the loss behavior for a transient to constant flux.

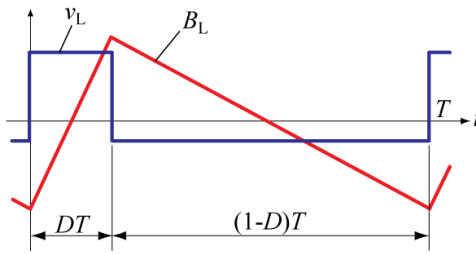


Fig. 8. Triangular flux density waveform.

This leads to a new model to calculate the time-average power loss density

$$P_v = \frac{1}{T} \int_0^T k_i \left| \frac{dB}{dt} \right|^\alpha (\Delta B)^{\beta-\alpha} dt + \sum_{l=1}^n P_{rl}, \quad (10)$$

where  $P_{rl}$  represents the time-average power loss density due to the  $l^{\text{th}}$  of  $n$  transients to zero voltage. This power loss of each transient to zero voltage is calculated according to

$$P_{rl} = \frac{1}{T} k_r \left| \frac{d}{dt} B(t_-) \right|^{\alpha_r} (\Delta B)^{\beta_r} \left( 1 - e^{-\frac{t_+}{\tau}} \right). \quad (11)$$

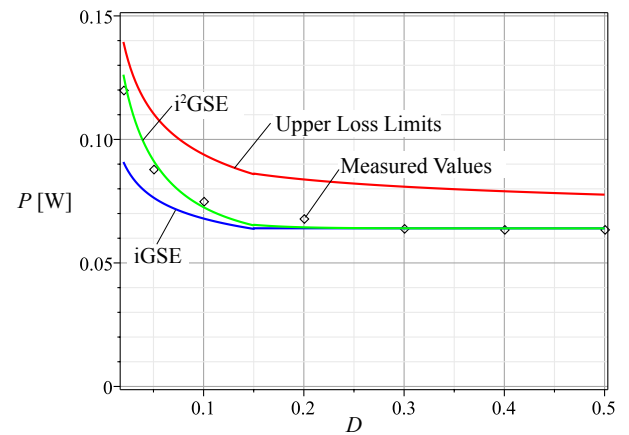
For the sake of completeness, a limitation of the given model should be pointed out. The curves in Fig. 6 do not have the shape of exact straight lines. This illustrates the fact that the newly introduced parameters  $\alpha_r$ ,  $\beta_r$  are only valid for a limited  $dB(t_-)/dt$  and  $\Delta B$  range. The limited parameter validity is a general problem of the Steinmetz approach.

## V. MODEL DERIVATION 2: TRIANGULAR FLUX WAVEFORM

Often in power electronics, one has a period of zero voltage applied to a magnetic component winding, e.g. in the transformer of a bidirectional isolated DC-DC converter with Dual Active full Bridges (DAB). A DAB will be presented in Section VII as an example to illustrate the model. In this case, (10) can directly be used to improve the loss model.

However, another frequently occurring waveform is a triangular flux waveform in which the flux slope changes to another nonzero value. This case is illustrated in Fig. 8. When a duty cycle of 50% ( $D = 0.5$ ) is assumed, directly after switching to the opposite voltage the flux slope reverses, the material has hardly time to move towards the new thermal equilibrium. As a consequence, no notable loss increase is expected and thus this case is well described by the iGSE (2). However, when the duty cycle goes to smaller values, once each period, a high flux slope is followed by a very slow flux change. Assuming  $D$  to be infinitely small, a switch to a constant flux happens. Consequently, in this case the iGSE (2) is not accurate and the relaxation term has to be added. In all operating points where  $D > 0$  and  $D < 0.5$  (or  $D > 0.5$  and  $D < 1$ ), a behavior that is in-between these two cases is expected. In other words, only part of the relaxation term has to be added.

In Fig. 9 the calculated and measured core losses as a function of the duty cycle are plotted. One calculation has been performed based on the iGSE (2) which, according to the above discussion, represents the lower limit of possible losses

Fig. 9. Core loss duty cycle dependency.  $\Delta B = 0.1$  T,  $f = 20$  kHz.

(as no relaxation effects are taken into account). It should be noted that two sets of Steinmetz parameters have been used for the calculation of the iGSE. The reason is that the Steinmetz parameters are only valid in a limited  $dB/dt$  range, and the  $dB/dt$  in this experiment is varying in a wide range. This explains the sharp bend of the iGSE curve at  $D = 0.15$  (change of Steinmetz parameter). Another calculation has been made always including the full relaxation loss term and which represents the upper loss loss limit. In other words, it can be said that losses are expected to have values between the line representing the upper loss limit and the line representing the lower loss limit (iGSE). According to the previous discussion, the real losses are closer to the lower loss limit for  $D$  close to 0.5, and losses closer to the upper loss limit for  $D$  close to zero. Measurements seem to confirm this hypothesis as can be seen in Fig. 9. Other operating points showed the same behavior.

Based on the above discussion, the new approach can be further improved to be also valid for triangular flux waveforms. Basically, (10) can be rewritten as

$$P_v = \frac{1}{T} \int_0^T k_i \left| \frac{dB}{dt} \right|^\alpha (\Delta B)^{\beta-\alpha} dt + \sum_{l=1}^n Q_{rl} P_{rl}, \quad (12)$$

where  $Q_{rl}$  has to be further defined. In the case of a switch to zero voltage,  $Q_{rl}$  needs to have the value 1. Furthermore, it has to have a structure such that (12) fits the measurement points of a duty cycle measurement, such as illustrated in Fig. 9. The following function has been chosen:

$$Q_{rl} = e^{-q_r \left| \frac{dB(t_+)/dt}{dB(t_-)/dt} \right|}, \quad (13)$$

where  $dB(t_-)/dt$  represents the flux density before the switching,  $dB(t_+)/dt$  the flux density after the switching, and  $q_r$  is a new material parameter. For a triangular waveform as illustrated in Fig. 8, (13) can be rewritten (for  $D \leq 0.5$ )

$$Q_{rl} = e^{-q_r \frac{\Delta B}{DT}} = e^{-q_r \frac{D}{1-D}}. \quad (14)$$

In the case of the material Epcos N87  $q_r = 16$  has been found, the resulting loss curve is plotted in Fig. 9. Before giving an

illustrative example in Section VII, the new model will be summarized and the steps to extract the model parameters will be given.

## VI. NEW CORE LOSS MODEL: THE $i^2GSE$

A new loss model that substantially increases the expected accuracy when core losses are modeled has been introduced. We call this new model the *improved-improved Generalized Steinmetz Equation*  $i^2GSE$ . The name has been chosen because it is an improved version of the  $iGSE$  [4]. The time-average power loss density can be calculated with

$$P_v = \frac{1}{T} \int_0^T k_i \left| \frac{dB}{dt} \right|^\alpha (\Delta B)^{\beta-\alpha} dt + \sum_{l=1}^n Q_{rl} P_{rl}, \quad (15)$$

where  $P_{rl}$  is calculated for each voltage change according to

$$P_{rl} = \frac{1}{T} k_r \left| \frac{d}{dt} B(t_-) \right|^{\alpha_r} (\Delta B)^{\beta_r} \left( 1 - e^{-\frac{t_1}{\tau}} \right), \quad (16)$$

$Q_{rl}$  is a function that further describes the voltage change and is

$$Q_{rl} = e^{-q_r \left| \frac{dB(t_+)/dt}{dB(t_-)/dt} \right|}, \quad (17)$$

and  $\alpha$ ,  $\beta$ ,  $k_i$ ,  $\alpha_r$ ,  $\beta_r$ ,  $k_r$ ,  $\tau$ , and  $q_r$  are material parameters.

Now, the steps to extract the model parameters are given:

- 1) First, the parameters  $k_i$ ,  $\alpha$ , and  $\beta$  are extracted. The core is excited with a rectangular voltage waveform that leads to a symmetric triangular flux waveform. Measurements at three operating points are performed, then (15) is solved for the three parameters. For symmetric triangular flux waveforms (with duty cycle  $D = 0.5$ ) it is  $\sum_{l=1}^n Q_{rl} P_{rl} = 0$ . In Table I the measurement results and the corresponding parameters are given. These parameters could be extracted directly from the data sheet as well, as explained in [4].
- 2) The parameter  $\tau$  can be read from Fig. 4 with

$$\frac{\Delta E}{\tau} = \frac{dE}{dt}, \quad (18)$$

where  $dE/dt$  represents the slope of the energy increase directly after switching to zero voltage. This is illustrated in Fig. 4.  $\tau = 6 \mu s$  has been extracted for the material N87.

- 3) The parameters  $k_r$ ,  $\alpha_r$ , and  $\beta_r$  are extracted by performing measurements at three operating points with  $t_1$  large enough to let the material reach the thermal equilibrium. Then, (9) is solved for the three parameters. In Table I the measurement results and the corresponding parameters are given.
- 4) The parameter  $q_r$  has to be selected such that (15) fits the measurement points of a duty cycle measurement, as illustrated in Fig. 9.

All model parameters are summarized in Table I. Extracting the parameters is sometimes difficult and measurements have to be performed very carefully. One error source is a possible current decrease due to a voltage drop over the inductor winding during "zero" voltage phase. This can be avoided by choosing a high amount of primary turns. This increases the

inductance value and the current is kept more constant (by choosing a high amount of primary turns the winding copper resistance increases as well, however, the inductance value increases quadratically while the resistance value increases linearly).

TABLE I  
MEASUREMENT RESULTS AND MODEL PARAMETER OF MATERIAL EPCOS N87.

Operating Point ( $\Delta B$ ; $f$ )	Loss Density [kW/m <sup>3</sup> ]	Model Parameters
(0.1 T; 20 kHz)	5.98	$k_i = 8.41$
(0.1 T; 50 kHz)	16.2	$\alpha = 1.09$
(0.2 T; 50 kHz)	72.8	$\beta = 2.16$
$(\Delta B; dB(t_-)/dt)$	[J/m <sup>3</sup> ]	
(0.1 T; 4 kT/s)	0.068	$k_r = 0.0574$
(0.1 T; 20 kT/s)	0.13	$\alpha_r = 0.39$
(0.2 T; 20 kT/s)	0.32	$\beta_r = 1.31$
		$\tau = 6 \mu s$
		$q_r = 16$

## VII. EXAMPLE OF HOW TO USE THE NEW MODEL

In the previous section, a new core loss modeling approach was introduced. This section shows now an easy-to-follow example that illustrates how to calculate core losses of a transformer employed in a bidirectional isolated DC-DC converter with Dual Active full Bridges (DAB) [6], [21]. In Fig. 10(a) the simplified schematic and in Table II the specifications of the transformer are given. The shape of the core influences the core losses, however, this is not the scope of the present work, hence a simple toroid is considered as the transformer core. Phase-shift modulation has been chosen as modulation method: primary and secondary full bridge switch with 50% duty cycle to achieve a rectangular voltage  $v_1$  and  $v_2$  across the primary and secondary transformer side, respectively. The waveforms are illustrated in Fig. 10(b), including the magnetic flux density  $B_\mu$  of the transformer core. A phase shift  $\gamma$  between  $v_1$  and  $v_2$  results in a power transfer. When the voltages  $v_1$  and  $v_2$  are opposed (which is the case in phase  $t_\gamma$ ), the full voltage drop is across the transformer leakage inductance and the magnetic flux density  $B_\mu$  remains unchanged.

Only the magnetic flux density  $B_\mu$  time behavior has been considered for designing the transformer, i.e. no winding losses or leakage inductance have been calculated. The value of the leakage inductance is very important for the functionality, however, it is not discussed here. Therefore, no statement about feasibility is made, the circuit should only represent solely a simple and easy-to-follow illustrative magnetic example.

The losses are calculated according to the  $i^2GSE$  (15). The results are then compared with measurement results. The peak flux density in the core can be calculated with [6]

$$\hat{B} = \frac{1}{2} \frac{V_{DC}}{NA_e} \left( \frac{T}{2} - t_\gamma \right) \quad (19)$$

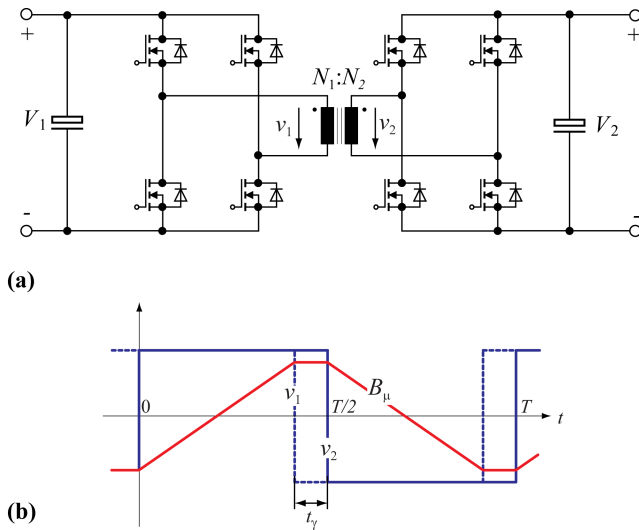


Fig. 10. DAB schematic (a) and waveforms (b) with specifications given in Table II.

TABLE II  
SPECIFICATIONS OF DAB TRANSFORMER

$V_{DC} = V_1 = V_2$	42 V
$f$	50 kHz
$N=N_1=N_2$	20
Effective Magnetic Length $l_e$	103 mm
Effective Magnetic Cross Section $A_e$	95.75 mm <sup>2</sup>
Core	EPCOS N87, R42 (B64290L22X87) [18]

and its time derivative with

$$\frac{dB}{dt} = \begin{cases} \frac{V_{DC}}{NA_e} & \text{for } t \geq 0 \text{ and } t < \frac{T}{2} - t_\gamma, \\ 0 & \text{for } t \geq \frac{T}{2} - t_\gamma \text{ and } t < \frac{T}{2}, \\ -\frac{V_{DC}}{NA_e} & \text{for } t \geq \frac{T}{2} \text{ and } t < T - t_\gamma, \\ 0 & \text{for } t \geq T - t_\gamma \text{ and } t < T. \end{cases} \quad (20)$$

Calculating the losses according to (15) leads to the following expression as a function of  $t_\gamma$

$$P = \frac{T - 2t_\gamma}{T} k_i \left| \frac{V_{DC}}{NA_e} \right|^\alpha \left| \frac{V_{DC}}{NA_e} \left( \frac{T}{2} - t_\gamma \right) \right|^{\beta-\alpha} A_{el} e + A_{el} e \sum_{l=1}^n Q_{rl} P_{rl}, \quad (21)$$

where  $\sum_{l=1}^2 Q_{rl} P_{rl}$  represents the two transients to zero voltage. There are two switching instants to zero voltage, each with  $Q_{rl} = 1$ . The values for  $P_{rl}$  then have to be determined: it is for each transient

$$P_{rl} = \frac{1}{T} k_r \left| \frac{V_{DC}}{NA_e} \right|^{\alpha_r} \left| \frac{V_{DC}}{NA_e} \left( \frac{T}{2} - t_\gamma \right) \right|^{\beta_r} \left( 1 - e^{-\frac{t_\gamma}{\tau}} \right). \quad (22)$$

The losses have been calculated according to the new approach, and have been compared to a calculation using the classic iGSE (2) and with measurement results. Open-circuit (no load) measurements have been performed to validate the new model: the primary winding is excited to achieve a flux

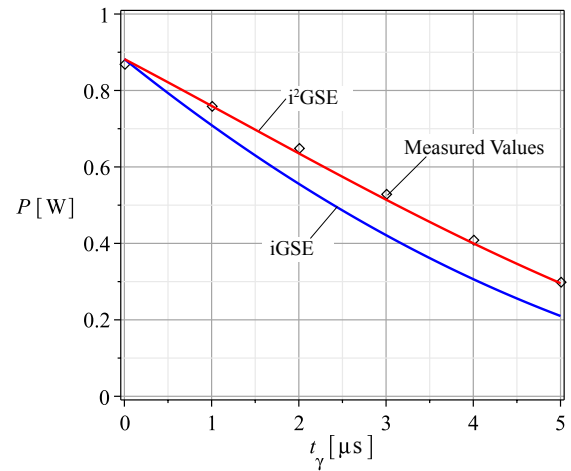


Fig. 11. Loss calculation and loss measurement comparison of the DAB example.

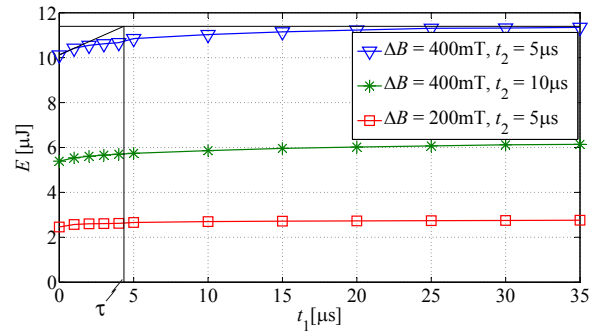


Fig. 12. Measurement results measured on VITROPERM 500F from VAC (measured on W452 core); temperature = 25 °C. It is further illustrated how  $\tau$  according to (18) can be extracted.

density as illustrated in Fig. 10(b). Measurements for different values of  $t_\gamma$  have been performed, at constant frequency  $f$  and voltage  $V_{DC}$ . The new model and measurement results match very well as shown in Fig. 11.

In [6] different state-of-the-art core loss calculation approaches are compared using a very similar example. The iGSE (2) showed the best agreement with measurements, but for increasing zero voltage periods  $t_\gamma$ , the calculated core losses start deviating from the measured core losses. The reason becomes clear with the new approach i<sup>2</sup>GSE and the calculation can be improved.

## VIII. MEASUREMENTS ON DIFFERENT MATERIALS

The approach has been confirmed on different materials, including on VITROPERM 500F from VAC (measured on W452 core). Measurements on waveforms as illustrated in Fig. 3(a) have been performed. Fig. 12 shows the corresponding measurement results. The model parameters are given in Table III. Measurements show promise that the approach is applicable for all material types; however, this remains to be confirmed as part of a future work.

TABLE III  
MODEL PARAMETER OF MATERIAL VITROPERM 500F (VAC).

$\alpha$	1.88
$\beta$	2.02
$k_i$	$137 \cdot 10^{-6}$
$\alpha_r$	0.76
$\beta_r$	1.70
$k_r$	$139 \cdot 10^{-6}$
$\tau$	$4.5 \mu\text{s}$
$q_r$	4

## IX. CONCLUSION AND FUTURE WORK

The Steinmetz Equation (1) and its extension iGSE (2) are relatively accurate models to describe core losses. However, some core loss mechanisms cannot be described with an equation of only three parameters. The Steinmetz parameters alone are insufficient to fully describe core losses. This publication together with the work presented in [17] try to show new approaches of how core losses could be better determined.

As experimentally verified, core losses are not necessarily zero when zero voltage is applied across a transformer or inductor winding after an interval of changing flux density. A short period after switching the winding voltage to zero, losses still occur in the material. This work hypothesizes that this is due to magnetic relaxation. A new loss modeling approach has been introduced and named the *improved-improved Generalized Steinmetz Equation*,  $i^2\text{GSE}$ . The  $i^2\text{GSE}$  needs five new parameters to calculate new core loss components. Hence, in total eight parameters are necessary to accurately determine core losses.

The tested measurement range is given in the following to identify the range in which the model validity has been confirmed. Two types of waveforms have been analyzed: trapezoidal as illustrated in Fig. 3(a) and triangular waveforms as illustrated in Fig. 8. For trapezoidal waveforms, measurements with  $t_1 = 0 \dots 500\mu\text{s}$  and  $t_2 = 5 \dots 100\mu\text{s}$  have been conducted. For the triangular waveforms measurements in the range between 20 kHz ... 100 kHz and  $D = 0.02 \dots 0.5$  have been conducted. No measurements for very low values of  $t_2$  have been conducted; however, the triangular operating point with  $D = 0.02$  and  $f = 20\text{ kHz}$ , for instance, has a flux rise time of  $1\mu\text{s}$ , which indicates that the model is also applicable for very short voltage pulses.

As stated in the introduction, the Steinmetz parameters are valid only for a limited frequency and flux density range. This is also the case for the additional parameters of the  $i^2\text{GSE}$  as has been illustrated in Fig. 6; however, this parameter dependency has not been further investigated for this work. Furthermore, a DC level of the antecedent flux density has not been part of this investigation of the present work and could be considered as part of a future work.

## ACKNOWLEDGEMENT

The authors would like to thank ABB Switzerland Ltd. for giving them the opportunity to work on this very interesting project.

## REFERENCES

- [1] E. C. Snelling, *Soft Ferrites, Properties and Applications*. 2<sup>nd</sup> edition, Butterworths, 1988.
- [2] J. Reinert, A. Brockmeyer, and R. De Doncker, "Calculation of losses in ferro- and ferrimagnetic materials based on the modified Steinmetz equation," *IEEE Transactions on Industry Applications*, vol. 37, no. 4, pp. 1055–1061, 2001.
- [3] J. Li, T. Abdallah, and C. R. Sullivan, "Improved calculation of core loss with nonsinusoidal waveforms," in *Industry Applications Conference, 2001. 36<sup>th</sup> IEEE IAS Annual Meeting*, vol. 4, pp. 2203–2210, 2001.
- [4] K. Venkatachalam, C. R. Sullivan, T. Abdallah, and H. Tacca, "Accurate prediction of ferrite core loss with nonsinusoidal waveforms using only Steinmetz parameters," in *Proc. of IEEE Workshop on Computers in Power Electronics*, pp. 36–41, 2002.
- [5] J. Biela, U. Badstuebner, and J. W. Kolar, "Impact of power density maximization on efficiency of DC-DC converter systems," *IEEE Transactions on Power Electronics*, vol. 24, pp. 288–300, Jan. 2009.
- [6] I. Villar, U. Viscarret, I. Etxeberria-Otadui, and A. Rufer, "Global loss evaluation methods for nonsinusoidally fed medium-frequency power transformers," *IEEE Transactions on Industrial Electronics*, vol. 56, pp. 4132–4140, Oct. 2009.
- [7] S. Iyasu, T. Shimizu, and K. Ishii, "A novel iron loss calculation method on power converters based on dynamic minor loop," in *Proc. of European Conference on Power Electronics and Applications*, pp. 2016–2022, 2005.
- [8] T. Shimizu and K. Ishii, "An iron loss calculating method for AC filter inductors used on PWM inverters," in *Proc. of 37<sup>th</sup> IEEE Power Electronics Specialists Conference (PESC)*, pp. 1–7, 2006.
- [9] K. Terashima, K. Wada, T. Shimizu, T. Nakazawa, K. Ishii, and Y. Hayashi, "Evaluation of the iron loss of an inductor based on dynamic minor characteristics," in *Proc. of European Conference on Power Electronics and Applications*, pp. 1–8, 2007.
- [10] J. B. Goodenough, "Summary of losses in magnetic materials," *IEEE Transaction on Magnetics*, vol. 38, pp. 3398–3408, Sept. 2002.
- [11] W. A. Roshen, "A practical, accurate and very general core loss model for nonsinusoidal waveforms," *IEEE Transactions on Power Electronics*, vol. 22, no. 1, pp. 30–40, 2007.
- [12] J. Liu, T. G. W. Jr., R. C. Wong, R. Wunderlich, and F. Lee, "A method for inductor core loss estimation in power factor correction applications," in *Proc. of Applied Power Electronics Conference and Exposition (APEC)*, 2002.
- [13] C. R. Sullivan, J. H. Harris, and E. Herbert, "Core loss predictions for general PWM waveforms from a simplified set of measured data," in *Proc. of Applied Power Electronics Conference and Exposition (APEC)*, pp. 1048–1055, 2010.
- [14] B. Carsten, "Why the magnetics designer should measure core loss; with a survey of loss measurement techniques and a low cost, high accuracy alternative," in *Proc. of PCIM*, pp. 163–179, 1995.
- [15] F. Dong Tan, J. Vollin, and S. Cuk, "A practical approach for magnetic core-loss characterization," *IEEE Transactions on Power Electronics*, vol. 10, pp. 124–130, Mar. 1995.
- [16] W. Shen, F. Wang, D. Boroyevich, and C. W. Tipton, "Loss characterization and calculation of nanocrystalline cores for high-frequency magnetics applications," *IEEE Transactions on Power Electronics*, vol. 23, pp. 475–484, Jan. 2008.
- [17] J. Mühlenthaler, J. Biela, J. W. Kolar, and A. Ecklebe, "Core losses under DC bias condition based on Steinmetz parameters," in *Proc. of the IEEE/IEEJ International Power Electronics Conference (ECCE Asia)*, pp. 2430–2437, 2010.
- [18] *Ferrites and Accessories, Edition 2007*. EPCOS AG.
- [19] G. Bertotti, *Hysteresis in Magnetism*. Academic Press, Inc., 1998.
- [20] S. Chikazumi, *Physics of Ferromagnetism*. Oxford University Press, 1997.
- [21] F. Krismer and J. W. Kolar, "Accurate power loss model derivation of a high-current dual active bridge converter for an automotive application," *IEEE Transactions on Industrial Electronics*, vol. 57, no. 3, pp. 881 – 891, 2010.



**Jonas Mühlthaler** (S'09) received his M.Sc. degree in electrical engineering from the Swiss Federal Institute of Technology (ETH) Zurich, Zurich, Switzerland, in 2008. During his studies, he focused on power electronics and electrical machines. In his M.Sc. thesis, which he wrote at ABB Corporate Research in Sweden, he worked on compensating torque pulsation in Permanent Magnet Motors. Since 2008 he is working toward the Ph.D. degree in the Power Electronic Systems Laboratory, focusing on modeling and designing magnetic components.



**Johann W. Kolar** (F'10) received his M.Sc. and Ph.D. degree (summa cum laude / promotio sub auspiciis praesidentis rei publicae) from the University of Technology Vienna, Austria. Since 1984 he has been working as an independent international consultant in close collaboration with the University of Technology Vienna, in the fields of power electronics, industrial electronics and high performance drives. He has proposed numerous novel converter topologies and modulation/control concepts, e.g., the VIENNA Rectifier, the Swiss Rectifier, and the

three-phase AC-AC Sparse Matrix Converter. Dr. Kolar has published over 400 scientific papers in international journals and conference proceedings and has filed more than 80 patents. He was appointed Professor and Head of the Power Electronic Systems Laboratory at the Swiss Federal Institute of Technology (ETH) Zurich on Feb. 1, 2001. The focus of his current research is on AC-AC and AC-DC converter topologies with low effects on the mains, e.g. for data centers, More-Electric-Aircraft and distributed renewable energy systems, and on Solid-State Transformers for Smart Microgrid Systems. Further main research areas are the realization of ultra-compact and ultra-efficient converter modules employing latest power semiconductor technology (SiC and GaN), micro power electronics and/or Power Supply on Chip Systems, multi-domain/scale modeling/simulation and multi-objective optimization, physical model-based lifetime prediction, pulsed power, and ultra-high speed and bearingless motors. He received the Best Transactions Paper Award of the IEEE Industrial Electronics Society in 2005, the Best Paper Award of the ICPE in 2007, the 1st Prize Paper Award of the IEEE IAS IPCC in 2008, the IEEE IECON Best Paper Award of the IES PETC in 2009, the 2009 IEEE Power Electronics Society Transaction Prize Paper Award, the 2010 Best Paper Award of the IEEE/ASME Transactions on Mechatronics, the Best Paper 1st Prize Award at the ECCE Asia 2011, and the 1st Place IEEE IAS Society Prize Paper Award 2011. He also received an Erskine Fellowship from the University of Canterbury, New Zealand, in 2003. He initiated and/or is the founder/co-founder of 4 spin-off companies targeting ultra-high speed drives, multi-domain/level simulation, ultra-compact/efficient converter systems and pulsed power/electronic energy processing. In 2006, the European Power Supplies Manufacturers Association (EPSMA) awarded the Power Electronics Systems Laboratory of ETH Zurich as the leading academic research institution in Power Electronics in Europe. Dr. Kolar is a Fellow of the IEEE and a Member of the IEEJ and of International Steering Committees and Technical Program Committees of numerous international conferences in the field (e.g. Director of the Power Quality Branch of the International Conference on Power Conversion and Intelligent Motion). He is the founding Chairman of the IEEE PELS Austria and Switzerland Chapter and Chairman of the Education Chapter of the EPE Association. From 1997 through 2000 he has been serving as an Associate Editor of the IEEE Transactions on Industrial Electronics and since 2001 as an Associate Editor of the IEEE Transactions on Power Electronics. Since 2002 he also is an Associate Editor of the Journal of Power Electronics of the Korean Institute of Power Electronics and a member of the Editorial Advisory Board of the IEEJ Transactions on Electrical and Electronic Engineering.



**Juergen Biela** (S'04 M'06) received the Diploma (with honors) from Friedrich-Alexander University (FAU) Erlangen, Nuremberg, Germany, in 1999 and the Ph.D. degree from the Swiss Federal Institute of Technology (ETH) Zurich, Zürich, Switzerland, in 2006. During his studies, he dealt in particular with resonant dc-link inverters at Strathclyde University, Glasgow, U.K., and the active control of series-connected IGCTs at the Technical University of Munich, München, Germany. From 2000, he was with the Research Department of A&D Siemens, Germany, where he worked on inverters with very high switching frequencies, SiC components, and EMC. In July 2002, he was with the Power Electronic Systems Laboratory (PES), ETH Zurich, while working toward the Ph.D. degree, focusing on optimized electromagnetically integrated resonant converter. From 2006 to 2007, he was a Postdoctoral Fellow with PES and has been a Guest Researcher at the Tokyo Institute of Technology, Tokyo, Japan. From 2007 to mid 2010, he was a Senior Research Associate with PES. In August 2010, he was appointed Associate Professor and Head of the Laboratory for High Power Electronic Systems at ETH Zurich. His current research is focused on design, modeling, and optimization of PFC, dc-dc, and multilevel converters with emphasis on SMART Grid, electric mobility and traction applications as well as pulsed-power systems for medical and accelerator applications.



**Andreas Ecklebe** (M'07) received the Dipl.-Ing. degree in electrical engineering in 2002 and the Dr.-Ing. degree in electrical engineering in 2009 both from the Otto-von-Guericke University, Magdeburg. From 2002 to 2004 he was with SMS Demag AG and Alstom Power Conversion, where he was engaged in the design of technological control systems for large scale industrial automation solutions. Since 2008 he is with ABB Corporate Research, Baden-Daettwil, Switzerland, where he is currently leading the Power Electronics Integration Research Group.